

METAL ABUNDANCES OF KISS GALAXIES I. COARSE METAL ABUNDANCES AND THE METALLICITY-LUMINOSITY RELATION.

JASON MELBOURNE¹ AND JOHN J. SALZER
 Astronomy Department, Wesleyan University, Middletown, CT 06459
 jmel@ucolick.org; slaz@astro.wesleyan.edu
To appear in the May, 2002 AJ

ABSTRACT

We derive metal abundance estimates for a large sample of starbursting emission-line galaxies (ELGs). Our sample is drawn from the KPNO International Spectroscopic Survey (KISS) which has discovered over 2000 ELG candidates to date. Follow-up optical spectra have been obtained for ~ 900 of these objects. A three step process is used to obtain metal abundances for these galaxies. We first calculate accurate nebular abundances for 12 galaxies whose spectra cover the full optical region from [OII] $\lambda\lambda 3726, 29$ to beyond [SII] $\lambda\lambda 6717, 31$ and include detection of [OIII] $\lambda 4363$. Using secondary metallicity indicators R_{23} and p_3 , we calculate metallicities for an additional 59 galaxies with spectra that cover a similar wavelength range but lack [OIII] $\lambda 4363$. The results are used to calibrate relations between metallicity and two readily observed emission-line ratios, which allow us to estimate coarse metallicities for 519 galaxies in total. The uncertainty in these latter abundance estimates is 0.16 dex. From the large, homogeneously observed sample of star-forming galaxies we identify low metallicity candidates for future study and investigate the metallicity-luminosity relation. We find a linear metallicity-luminosity relation of the following form: $12 + \log(\text{O}/\text{H}) = 4.059 - 0.240 M_B$, with an RMS scatter of 0.252. This result implies that the slope of the metallicity-luminosity relation is steeper than when dwarf galaxies are considered alone, and may be evidence that the relationship is not linear over the full luminosity range of the sample.

Subject headings: galaxies: abundances — galaxies: evolution — galaxies: starburst

1. INTRODUCTION

Observing metal abundances in galaxies is a valuable probe of galaxian star-formation histories and chemical evolution. Assuming that all galaxies begin with the same primordial abundances of elements, roughly 75% hydrogen and 25% helium, measurements of heavier elements indicate subsequent star formation accompanied by supernova explosions which enrich their surroundings with metals. Recent studies show that metallicity is linked with galaxy luminosity (Skillman et al. 1989; Zaritsky et al. 1994; Richer and McCall 1995; Garnett et al. 1997; Hunter and Hoffman 1999; Pilyugin and Ferrini 2000; Pilyugin 2001b) in that more luminous galaxies tend to be more metal rich than less luminous galaxies. This may indicate an evolutionary trend with several possible explanations. For example, a simple closed box model gives rise to such a trend (Hidalgo-Gamez and Olofsson 1998). Alternatively, evidence for large disruptions in the gas content of galaxies from supernova explosions may play a significant role. Specifically, supernovae have been proposed as a mechanism for removing large amounts of metal-enriched gas from low-mass systems (e.g., Mac Low and Ferrara 1999). This in turn may explain the relative dearth of metals in dwarf galaxies. In addition, higher astration levels in more luminous galaxies may contribute to their increased metallicity per mass (Pilyugin and Ferrini 2000).

The KPNO International Spectroscopic Survey (KISS) has identified over 2000 emission-line galaxy (ELG) candidates ranging in absolute magnitude from $M_B = -22$ to -12 (Salzer et al. 2000, 2001). As such, it provides a large sam-

ple of galaxies for which metallicities can be derived and from which the metallicity-luminosity relation can be studied. The survey lists include massive starburst-nucleus galaxies, intermediate-mass irregular galaxies, low-mass dwarf irregulars and blue compact dwarfs. In this work we derive coarse metallicity estimates for the 519 starburst galaxies which have adequate quality follow-up spectra. The results provide a list of low metallicity candidates for future study as well as the largest sample of galaxies to date for use in studying the metallicity-luminosity relation.

Most previous studies of the metallicity-luminosity relation have concentrated on low metallicity galaxies where accurate abundances are readily available. Studies of irregulars with current star formation (Skillman et al. 1989; Richer and McCall 1995) show evidence for a linear relation. However, another recent study of dwarf irregulars (Hidalgo-Gamez and Olofsson 1998) does not support these results. In re-examining the Hidalgo-Gamez and Olofsson data, Pilyugin (2001b) believes that noise in the [OIII] $\lambda 4363$ line is responsible for the lack of a relation in their sample.

On the high mass end, Garnett et al. (1997) compiled a data set of 29 luminous spirals, with metallicities derived from HII regions. The data set is taken from Vila-Costas and Edmunds (1992), Zaritsky et al. (1994) and Ryder (1995). They find that these more massive galaxies follow a similar trend to dwarf irregulars of increasing metallicity with luminosity. Garnett et al. do not offer a specific fit to the relation, but rather state that the high luminosity result maps smoothly onto the dwarf irregular relations such as that of Skillman et al. The same conclusions are drawn

¹ Present address: Department of Astronomy and Astrophysics, University of California, Santa Cruz, Santa Cruz, CA 95064

by Zaritsky et al. (1994). Pilyugin and Ferrini (2000) combine the low and high mass galaxy samples to provide a new fit to the metallicity-luminosity relation and show a somewhat steeper relation than Skillman et al (1989).

By using the large KISS sample of galaxies we investigate whether the metallicity-luminosity relation is actually present on all mass, luminosity and metallicity scales. Our abundance determinations are coarse and we use all morphological types for our metallicity-luminosity relation. Therefore our relation contains significantly more scatter than previous results. However, our luminosity range goes three magnitudes brighter than most previous studies, and we use up to 20 times more galaxies, giving us a better view of the overall form of the metallicity-luminosity relation, as well as its intrinsic scatter. We confirm the existence of a metallicity-luminosity relation that varies smoothly from massive luminous galaxies, $M_B < -21$, to blue compact dwarfs, $M_B > -16$. However, when the metallicity-luminosity relationship is calculated using the wide range of galaxy types found in the KISS sample, the slope of the relation is steeper than indicated by the studies of dwarf galaxies such as Skillman et al. and Richer and McCall. As a result we find that a simple extrapolation of the dwarf galaxy relationship to more massive systems is inappropriate. This may be an indication that the overall form of the metallicity-luminosity relation is not linear but rather requires a higher order polynomial to fit the data. It may also indicate that different galaxy types obey different metallicity-luminosity relations.

2. OBSERVATIONS AND DATA REDUCTION

2.1. Observations

Drawing from the KISS sample of emission-line galaxies, we gathered both imaging and spectral data for ~ 900 galaxies over a four year period from 1998 - 2001. Photometry is presented in the survey lists (Salzer et al. 2001; 2002a; Gronwall et al. 2002a) while results of spectral follow-up are given in a series of papers (Melbourne et al. 2002, hereafter Paper II; Salzer et al. 2002b; Wegner et al. 2002). A summary of the overall spectroscopic properties of the KISS ELGs will be presented in Gronwall et al. (2002b).

The spectral data can be classified into 3 groups based on spectral coverage and quality. Group I spectra, an example of which is given in Figure 1a, cover the full optical region from $[\text{OII}]\lambda\lambda 3726, 29$ to beyond $[\text{SII}]\lambda\lambda 6717, 31$ and contain the $[\text{OIII}]\lambda 4363$ line necessary for accurate abundance measurements. Abundances are calculated for Group I galaxies using the $[\text{OIII}]\lambda 4363$ line as an electron temperature indicator. All 12 objects in this group were observed with the Lick 3m telescope. The spectroscopic data and abundance analysis are presented in detail in Paper II.

Group II data also cover the full optical region from $[\text{OII}]\lambda\lambda 3726, 29$ to beyond $[\text{SII}]\lambda\lambda 6717, 31$, but do not necessarily contain the $[\text{OIII}]\lambda 4363$ line needed for accurate abundance measurements. Metal abundance estimates are derived from the strong oxygen lines $[\text{OII}]\lambda\lambda 3726, 29$ and $[\text{OIII}]\lambda\lambda 4959, 5007$ using the secondary metallicity indicators R_{23} (Pagel et al. 1979) and p_3 (Pilyugin 2000). The data were obtained at the Lick 3m, the APO 3.5m and KPNO 2.1m telescopes and include 59 additional objects.

A sample spectrum is shown in Figure 1b.

Group III spectra do not reach blueward to the $[\text{OII}]\lambda\lambda 3726, 29$ line. Metal abundances are derived for these galaxies based on empirical relations between the $[\text{OIII}]\lambda 5007/\text{H}\beta$ line ratio and metallicity and the $[\text{NII}]\lambda 6583/\text{H}\alpha$ line ratio and metallicity. Data in this category were obtained from the above mentioned telescopes as well as the WYN 3.5m, the MDM 2.4m and the Hobbey-Eberly 9m (HET). As the HET is a 9m-class telescope, the spectra have a high signal-to-noise ratio as shown in Figure 1c. Unfortunately, they do not extend much bluer than $\text{H}\gamma$. The $[\text{SII}]$ doublet on the red side is also often beyond the wavelength range of the spectrograph. The MDM images have a low dispersion. Therefore, as is shown in Figure 1d, the $[\text{NII}]\lambda 6583$ line blends with $\text{H}\alpha$, and the $[\text{SII}]\lambda\lambda 6717, 31$ doublet is also blended.

Details of the observations, data reduction methods and line measurements are given in a series of papers which present the results of our extensive spectroscopic follow-up (Paper II; Salzer et al. 2002b; Wegner et al. 2002).

3. METALLICITIES OF KISS GALAXIES

The most accurate calculation of metallicity in nebular star-forming regions uses the $[\text{OIII}]\lambda 4363$ line to measure the electron gas temperature (Osterbrock 1989; Izo-tov et al. 1994). This method, referred to here as the T_e method, works well for low metallicity systems (generally $12 + \log(\text{O}/\text{H}) < 8.2$) where the $[\text{OIII}]\lambda 4363$ line is observable. For systems of higher metallicity, $[\text{OIII}]\lambda 4363$ is often too weak to observe or too noisy to be trusted. However, the strong nebular lines alone contain the necessary information to arrive at relatively good estimates of the oxygen abundances in star-forming regions (Pagel et al. 1979; McGaugh 1991; Pilyugin 2000). The traditional R_{23} method (Edmunds and Pagel 1984) typically results in metallicities within 0.2 dex of the more exact T_e abundances. Pilyugin (2000) improves on the standard R_{23} method by introducing his p_3 factor calculated from the strong oxygen lines. The p_3 factor replaces the temperature as a descriptor of the conditions in the nebula and allows his method to correlate with the T_e method to within 0.1 dex for starbursts with metallicities below $12 + \log(\text{O}/\text{H}) < 7.9$. In this section we make use of the T_e , R_{23} and p_3 methods to estimate metallicities for 71 KISS galaxies. These data are then used to show that both the $[\text{OIII}]\lambda 5007/\text{H}\beta$ and $[\text{NII}]\lambda 6583/\text{H}\alpha$ line ratios correlate with metal abundance. We use the relationships to estimate coarse metallicities for the large, homogeneously observed KISS sample of galaxies. The details of each step follow.

3.1. T_e Metallicities

Spectra of 12 KISS galaxies contain the necessary information for high quality metal abundance determinations. Following the standard procedure (Osterbrock 1989; Izo-tov et al. 1994) we calculate the electron density from the $[\text{SII}]$ line ratio, and the electron temperature from the $[\text{OIII}]$ line ratio. Metal abundances are derived using the IRAF NEBULAR package (de Robertis et al. 1987; Shaw et al. 1995). Details of the observations, data reductions and analysis are given in Paper II. The results are presented in Table 1. We use the T_e abundance results in

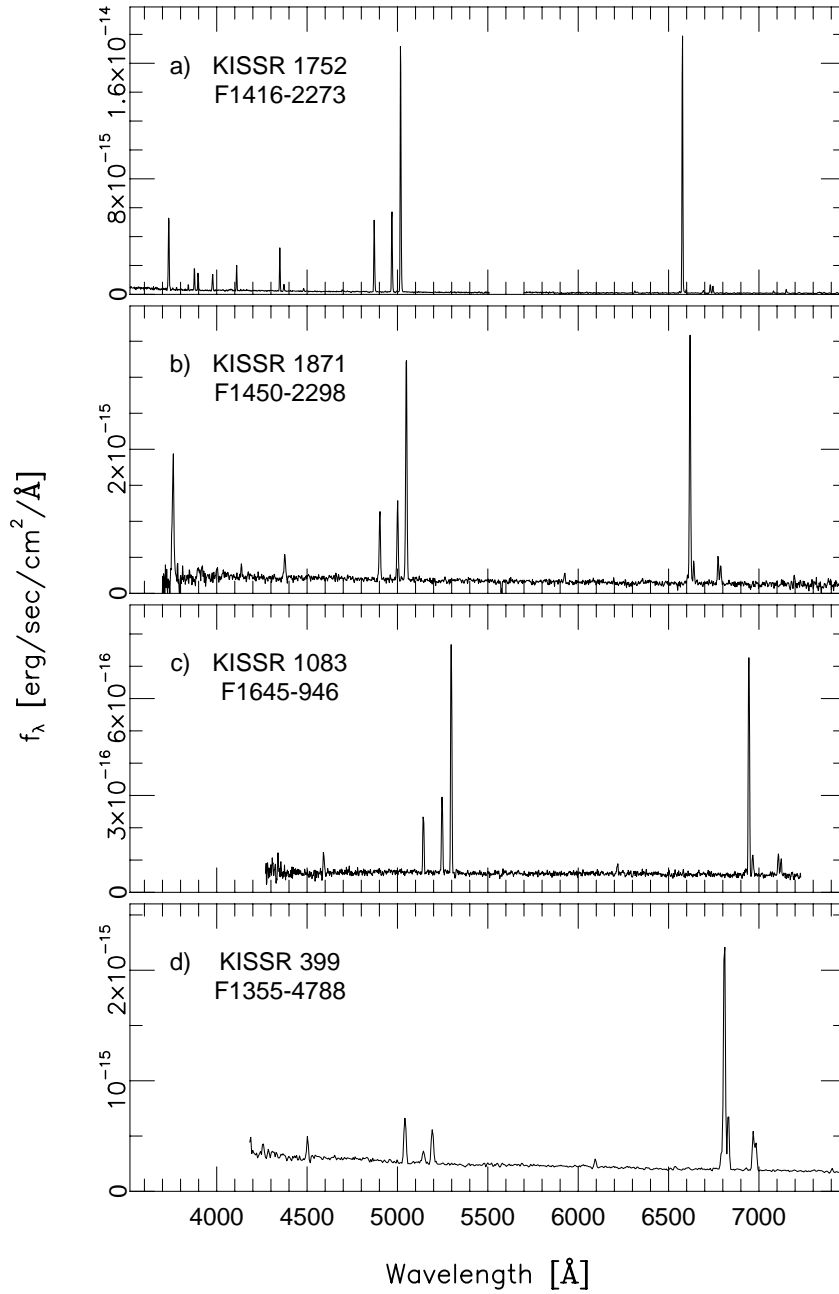


FIG. 1.— Sample spectra from the KISS archive: a) A Group I spectrum taken at the Lick 3m telescope. It covers the full optical region from [OII] $\lambda\lambda 3726,29$ to beyond [SII] $\lambda\lambda 6717,31$ and includes detection of the [OIII] $\lambda 4363$ line necessary for accurate metal abundances. b) A Group II spectrum taken at the Kitt Peak 2.1m telescope. It also covers the full optical region but does not have the signal-to-noise ratio necessary for the detection of [OIII] $\lambda 4363$. c) A Group III spectrum taken with the HET 9m telescope. It has a high signal-to-noise ratio because of the large telescope aperture, but does not cover the full optical region and is specifically lacking [OII] $\lambda\lambda 3726,29$. d) Also a group III spectrum, taken with the MDM 2.4m. It has lower dispersion; the nitrogen lines are blended with H α , and the sulfur doublet is also blended.

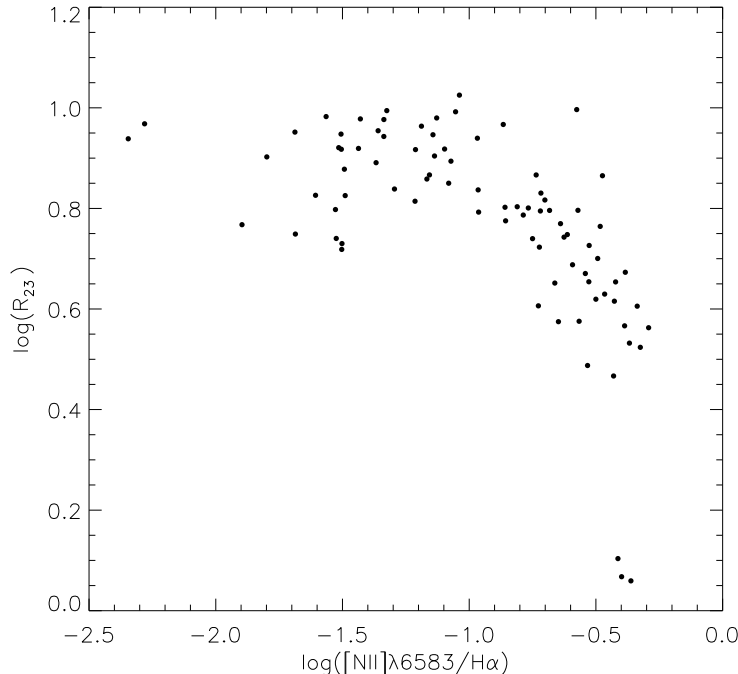


FIG. 2.— This line diagnostic diagram shows the relationship between R_{23} and the $[\text{NII}]\lambda 6583/\text{H}\alpha$ line ratio. Metallicity varies smoothly along the observed distribution, with high metallicity galaxies to the lower right and low metallicity galaxies to the upper left. When $\log([\text{NII}]\lambda 6583/\text{H}\alpha) < -1.3$ the galaxy is on the low metallicity branch of the R_{23} parameter. When $-1.3 < \log([\text{NII}]\lambda 6583/\text{H}\alpha) < -1.0$ the galaxy is in the turn around region, and when $\log([\text{NII}]\lambda 6583/\text{H}\alpha) > -1.0$ the galaxy is the high metallicity branch of the R_{23} parameter.

Section 3.3 when we correlate metallicity with emission-line ratios.

3.2. Secondary Metallicity Indicators R_{23} and p_3

The strong oxygen lines $[\text{OIII}]\lambda\lambda 4959, 5007$ and $[\text{OII}]\lambda\lambda 3726, 29$ contain the necessary information to predict the metallicity of an HII region (Pagel et al. 1979; McGaugh 1991). Traditionally this has been done by invoking the R_{23} parameter (Pagel et al. 1979), where;

$$R_{23} = \frac{f([\text{OIII}]\lambda 4959 + \lambda 5007) + f([\text{OII}]\lambda 3726 + \lambda 3729)}{f(\text{H}\beta)}. \quad (1)$$

The R_{23} parameter has been correlated with metallicity by measuring oxygen abundances *via* the T_e method for large samples of galaxies and HII regions. A complication with this method is that the dependence of metallicity on R_{23} is double valued. On the low metallicity end, $12 + \log(\text{O}/\text{H}) < 7.9$, R_{23} increases with metallicity. As the amount of oxygen in the nebula increases the strength of the emission leaving the nebula in the forbidden oxygen lines also increases. For higher metallicities, $12 + \log(\text{O}/\text{H}) > 8.1$, R_{23} decreases with increasing metallicity. In this case the majority of the energy leaves the nebula in other nebular lines. Between the high and low metallicity branches is the “turn-around region” where R_{23} ceases to be a good predictor of metallicity. In the “turn-around region” galaxies with the same R_{23} ratio can have a fairly wide range of metallicities.

We distinguish between the upper and lower branches of the R_{23} relation by observing the $[\text{NII}]\lambda 6583/\text{H}\alpha$ line ratio. This is demonstrated in Figure 2, a line diagnos-

tic diagram plotting $\log(R_{23})$ vs. $\log([\text{NII}]\lambda 6583/\text{H}\alpha)$. In this plot, metallicity varies smoothly across the figure with low abundance galaxies found in the upper left hand corner and high abundance galaxies in the lower right. We adopt the following criteria for determining on which branch of the R_{23} relation a given spectrum lies. We assign objects with $\log([\text{NII}]\lambda 6583/\text{H}\alpha) < -1.3$ to the low metallicity branch of the R_{23} relation. Objects with $\log([\text{NII}]\lambda 6583/\text{H}\alpha) > -1.0$ are associated with the high metallicity branch. Objects with $-1.3 < \log([\text{NII}]\lambda 6583/\text{H}\alpha) < -1.0$ are considered turn around region objects. We do not calculate R_{23} metallicities for these galaxies.

Unfortunately R_{23} does not correlate perfectly with metallicity. Galaxies with a given value for R_{23} can exhibit a range of T_e -method-determined metallicities. Other factors have been found to account for the variations. The spread in metallicity, especially on the low metallicity end, for a given R_{23} value is due to both to uncertainty/scatter in the T_e calibration and to additional parameters such as the initial mass function (IMF) of the starburst and density variations in the nebula (McGaugh 1991). The spread in metallicities for a given value of R_{23} at the high metallicity end is due primarily to a lack of good T_e abundance measurements.

A recent paper by Pilyugin (2000) demonstrates a method to remove R_{23} ’s density and IMF dependencies at the low metallicity end. Pilyugin defines a new parameter, $p_3 = X_3 - X_{23}$, where $X_3 = \log(f([\text{OIII}]\lambda 4959 + \lambda 5007)/f(\text{H}\beta))$ and $X_{23} = \log(R_{23})$. If the measure of X_{23} is constant for HII regions of similar oxygen abundance,

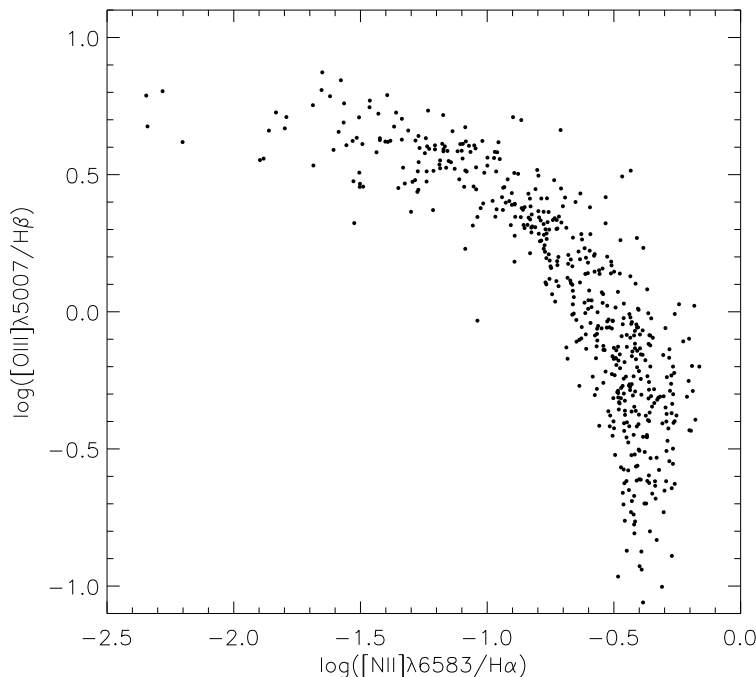


FIG. 3.— This line diagnostic diagram shows the relationship between the $[\text{NII}]\lambda 6583/\text{H}\alpha$ line ratio and the $[\text{OIII}]\lambda 5007/\text{H}\beta$ line ratio. High metallicity galaxies are found on the lower right where the oxygen line ratio is a good predictor of metallicity. Low metallicity galaxies are found to the upper left where the nitrogen line ratio is a good metallicity indicator.

then a plot of p_3 vs. X_3 should give a line with a slope of 1 for objects of the same metallicity. When Pilyugin plotted several HII regions in this way, he found the slope is not 1, implying that X_{23} can vary for objects with the same oxygen abundance. He defined a parameter, X_3^* , which is equal to the value of X_3 when the data in the X_3 vs. p_3 plot are extrapolated to $p_3 = 0$. Doing so he found the following relation:

$$X_3^* = X_3 - 2.20p_3. \quad (2)$$

For any observed value of X_3 and p_3 one can calculate X_3^* . Pilyugin goes on to demonstrate a correlation between X_3^* and metallicity which agrees with the T_e method to within 0.1 dex. The p_3 method effectively removes the systematic uncertainties in the R_{23} method on the low metallicity end. As he describes it, the temperature measurement in the T_e method accounts for the state of the IMF and the geometry factors in the nebula. In this new method, p_3 replaces the temperature as a descriptor of these influences. The correlation Pilyugin found which we will adopt for objects on the lower metallicity branch of the R_{23} relation is given in by the following equation:

$$12 + \log(\text{O}/\text{H}) = 6.35 + 1.45X_3^*. \quad (3)$$

Pilyugin (2001a) derives a similar relation for the upper metallicity branch. Unfortunately it is of use only in a limited metallicity range (~ 8.1 to ~ 8.6 dex). In addition, fits to the upper branch suffer more from a lack of good calibration points than from a multi-valued R_{23} relation. For simplicity we will adopt the Edmunds and Pagel (1984) fit to the upper branch. This fit, as quoted in Pilyugin (2000), can be expressed as follows:

$$12 + \log(\text{O}/\text{H}) = 9.57 - 1.38\log(R_{23}). \quad (4)$$

With the two methods, R_{23} and p_3 , we determine metallicities for galaxies which possess spectra that contain both the strong $[\text{OIII}]\lambda\lambda 4959, 5007$ and the strong $[\text{OII}]\lambda\lambda 3726, 29$. When $\log([\text{NII}]\lambda 6583/\text{H}\alpha) < -1.3$, we use p_3 to derive metallicity. When $\log([\text{NII}]\lambda 6583/\text{H}\alpha) > -1.0$ we use R_{23} to derive metallicity. For galaxies with $-1.3 < \log([\text{NII}]\lambda 6583/\text{H}\alpha) < -1.0$ we can not use either method as the object is in the turn-around region.

As an additional consideration, small uncertainties in the reddening coefficient, $c_{H\beta}$, can translate to large errors in the $[\text{OII}]\lambda 3726 + \lambda 3729/\text{H}\beta$ line ratio. Therefore metallicities derived with the strong-line method can be influenced by weak or noisy H β lines. For example, if we plot $\log([\text{OIII}]\lambda 4959 + \lambda 5007/[\text{OII}]\lambda 3726 + \lambda 3729)$ vs. $\log(R_{23})$ (McGaugh 1991) for our sample of galaxies, we find several objects in unphysical locations of the diagram. When we plot the same diagram restricting our sample of objects to those with an equivalent width of H β greater than 8 Å, the discrepant points are removed. Therefore, to ensure good spectral quality and accurate line ratios, we have adopted an H β equivalent width limit of 8 Å for the ensuing analysis.

With the equivalent width limit of H β and the nitrogen line ratio criteria specified, we calculate metallicities for 59 additional galaxies, 46 using the R_{23} method and 13 using the p_3 method. The metallicities for these galaxies along with the oxygen line ratios are given in Tables 2 and 3. We also have p_3 abundances for the twelve Group I galaxies that have T_e metallicities. Seven of the galaxies have p_3 abundances within 0.1 dex of their T_e result. Four are within 0.2 dex and one galaxy is highly deviant at 0.4 dex. We believe the reason for the deviation is related to the evolutionary state of the starburst. This particular galaxy

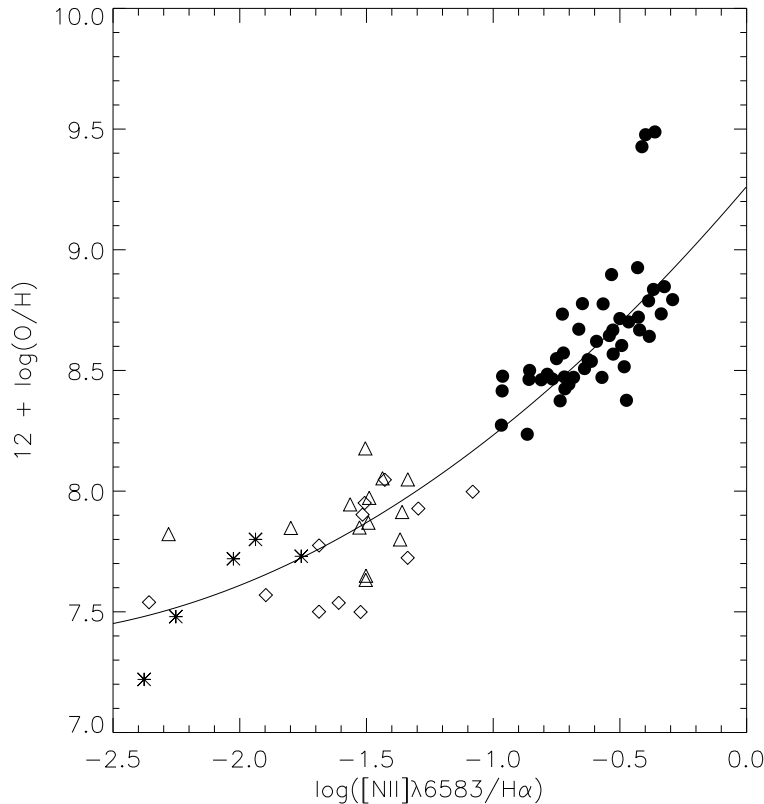


FIG. 4.— This line diagnostic diagram relates the $[\text{NII}]\lambda 6583/\text{H}\alpha$ line ratio to metallicity. Abundances calculated using the R_{23} fit are shown as circles, while p_3 abundances are shown as triangles. Abundances calculated with the T_e method are shown as diamonds. T_e abundance data taken from Izotov et al. (1997) are shown as '*'s. We fit a quadratic function to the data (solid line, see text).

appears to be a highly evolved, low-metallicity starburst. Since it is well past the peak of its star formation episode, it has an elevated $[\text{OII}]\lambda 3726 + \lambda 3729/\text{H}\beta$ line ratio despite the low overall metal abundance. The Pilyugin fit may not track this evolution as his fit is based on the relatively young starbursts studied by Izotov et al. (1997; 1998; 1999). Further comparison of the two methods will be presented in Paper II. When calibrating the low metallicity end of our line diagnostic diagrams, we will use the T_e abundances when available and the p_3 abundances for objects with no T_e result.

3.3. Metallicities from Line-Diagnostic Diagrams

We use the R_{23} , p_3 and T_e metallicities presented in the previous sections to relate the $[\text{OIII}]\lambda 5007/\text{H}\beta$ and $[\text{NII}]\lambda 6583/\text{H}\alpha$ line ratios with metallicity. We choose these two line ratios because they are observed in nearly all of our ELGs, typically have good signal-to-noise ratios, and are fairly insensitive to uncertainties in reddening corrections. We find that both the $[\text{OIII}]\lambda 5007/\text{H}\beta$ and $[\text{NII}]\lambda 6583/\text{H}\alpha$ line ratios can be used as predictors of metallicity. However, they both have limitations. A plot of the relationship between $\log([\text{OIII}]\lambda 5007/\text{H}\beta)$ and $\log([\text{NII}]\lambda 6583/\text{H}\alpha)$ is given in Figure 3. In this plot, metallicity varies smoothly over the distribution of galaxies with low metallicity systems in the upper left and high metallicity galaxies in the lower right. At the low metallicity end, the $[\text{OIII}]\lambda 5007/\text{H}\beta$ line remains almost constant for a large range of $\log([\text{NII}]\lambda 6583/\text{H}\alpha)$ values. Specifically, for

$\log([\text{NII}]\lambda 6583/\text{H}\alpha) < -1.2$ the $[\text{OIII}]\lambda 5007/\text{H}\beta$ line ratio is not a good metallicity indicator. Similarly, on the high metallicity end the $[\text{NII}]\lambda 6583/\text{H}\alpha$ line ratio ceases to be a good metallicity indicator for $\log([\text{OIII}]\lambda 5007/\text{H}\beta) < -0.25$ (see also Figure 2). We will use this information to decide which line ratio provides the most accurate metal abundance for a given galaxy.

In Figure 4 we plot $\log([\text{NII}]\lambda 6583/\text{H}\alpha)$ vs. metallicity for the Group I and II data. As the data are sparse on the low metallicity end we supplement with T_e results taken from the literature (Izotov et al. 1997). The diagram shows that metallicity increases with nitrogen line strength as a smooth single valued function up to the metal rich end of the distribution. At $\log([\text{NII}]\lambda 6583/\text{H}\alpha) > -0.45$ there is a sharp upturn in the observed distribution. This corresponds to the regime where the nitrogen line ratio ceases to be a good metallicity indicator, precisely the phenomenon seen in Figures 2 and 3. We fit a quadratic function to the data points with $\log([\text{NII}]\lambda 6583/\text{H}\alpha) < -0.45$ and obtain the following result:

$$12 + \log(\text{O}/\text{H}) = 9.26 + 1.23N + 0.204N^2, \quad (5)$$

$$N = \log([\text{NII}]\lambda 6583/\text{H}\alpha).$$

The data points have a root-mean-square (RMS) scatter about the fit of 0.156 dex. We use Equation 5 to estimate the metallicity for galaxies with $\log([\text{OIII}]\lambda 5007/\text{H}\beta) > -0.25$.

In Figure 5 we plot $\log([\text{OIII}]\lambda 5007/\text{H}\beta)$ vs metallicity for the Group I and II data. The relation is well defined at the high metallicity end. On the low metallicity end, we

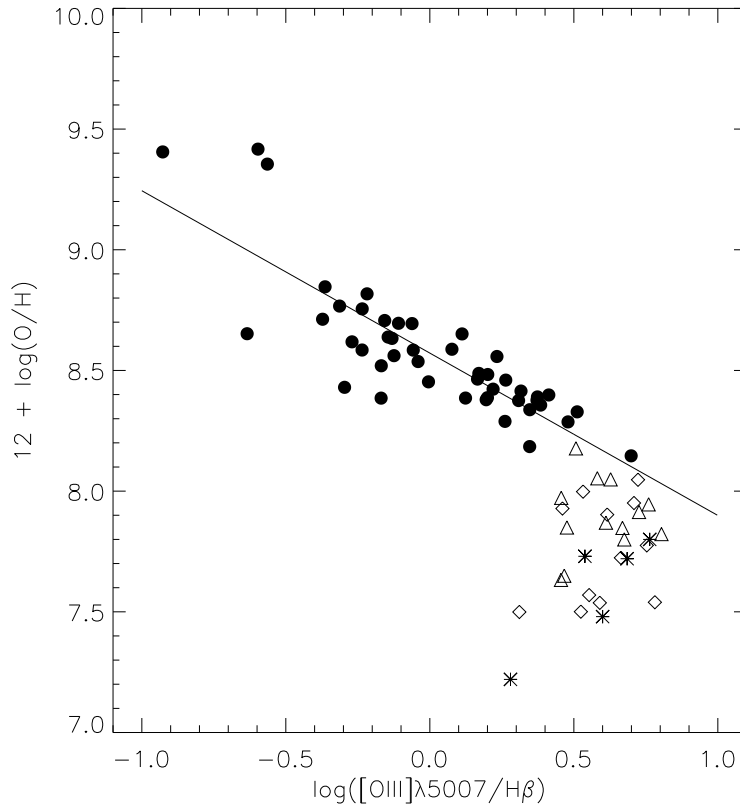


FIG. 5.— This line diagnostic diagram relates the $[\text{OIII}]\lambda 5007/\text{H}\beta$ line ratio to metallicity. Abundances calculated using the R_{23} fit are shown as circles, while p_3 abundances are shown as triangles. Abundances calculated with the T_e method are shown as diamonds. T_e abundance data taken from Izotov et al. (1997) are shown as '*'s. We fit a line to the high metallicity branch (solid line, see text).

see a scattered clump of galaxies with metallicities ranging from 7.5 to 8.2 dex and $\log([\text{OIII}]\lambda 5007/\text{H}\beta)$ ranging from 0.3 to 0.8. Again we see that $[\text{OIII}]\lambda 5007/\text{H}\beta$ is not a good indicator of metallicity for low metallicity systems as predicted by Figure 3. We fit a linear function to all points on the upper metallicity branch, where $\log([\text{NII}]\lambda 6583/\text{H}\alpha) > -1.2$. We ignore objects in the turn-around region and below. The result for the fit is as follows:

$$12 + \log(\text{O}/\text{H}) = 8.65 - 0.663 O_x \quad (6)$$

$$O_x = \log([\text{OIII}]\lambda 5007/\text{H}\beta),$$

with an RMS of 0.149 dex. We use Equation 6 to estimate metallicities for KISS galaxies with $\log([\text{NII}]\lambda 6583/\text{H}\alpha) > -1.2$.

We use Equations 5 and 6 to compute final metallicity estimates for all KISS ELGs with the necessary spectral information available. Included are all objects that possess follow-up spectra rated as good or excellent quality, that have been classified as starbursting ELGs, and for which measurements of both $[\text{NII}]\lambda 6583/\text{H}\alpha$ and $[\text{OIII}]\lambda 5007/\text{H}\beta$ exist. A total of 519 galaxies satisfy these criteria. For a number of galaxies, metallicity estimates are computed using a single line ratio, while for others both line ratios are used. We combine the nitrogen and oxygen metallicity results in the following way. Referring again to Figure 3, for galaxies with $\log([\text{NII}]\lambda 6583/\text{H}\alpha) < -1.2$ we calculate the metallicity using only the nitrogen line ratio and Equation 5. For objects with $\log([\text{OIII}]\lambda 5007/\text{H}\beta) < -0.25$, we use only the oxygen line ratio and Equation 6 to calculate metal-

licity. For galaxies with $\log([\text{NII}]\lambda 6583/\text{H}\alpha) > -1.2$ and $\log([\text{OIII}]\lambda 5007/\text{H}\beta) > -0.25$ we calculate metallicities using both the nitrogen and oxygen line ratios and Equations 5 and 6. We take the average of the two results to produce a final abundance estimate. When we have estimates of the metallicity from both the nitrogen and oxygen line ratios, we find that the RMS scatter in the difference of the two measurements is 0.13, but that the mean difference is -0.009 (i.e., consistent with zero difference).

This process generates metallicity estimates for 519 homogeneously observed starbursting galaxies out to a redshift of $z=0.095$. Since the RMS scatter in Equations 5 and 6 is 0.156 and 0.149 respectively, we assign a uncertainty of 0.16 dex to each metallicity measurement. To be conservative, we use this uncertainty even when averaging two metallicity estimates together. Abundance estimates for individual galaxies calculated from these empirical methods will be tabulated in Gronwall et al. (2002b). Here we use the results to identify low metallicity candidates for further study. A list of objects with metallicities below 7.9 is given in Table 4. Several of these objects have been observed in detail with the Lick telescope (Paper II) but many more warrant high signal-to-noise ratio observations yielding T_e abundance data. As the objects in Table 4 are low metallicity, high quality abundance measurements of these galaxies can be used to study the primordial helium abundance (Izotov et al. 1994; 1997) and place constraints on Big Bang nucleosynthesis. In the next section, this large sample of data will be used to investigate the existence and form of the metallicity-luminosity relation.

4. THE METALLICITY-LUMINOSITY RELATIONSHIP

We combine galaxy metallicity estimates with calculations of the absolute B magnitudes to investigate the form of the metallicity-luminosity relationship. Apparent magnitudes, corrected for galactic reddening, are measured from the imaging portion of the survey data. We adopt a Hubble constant of $H_0 = 75 \text{ km} \cdot \text{s}^{-1} \cdot \text{Mpc}^{-1}$, and use the redshift measured from the follow-up spectrum of each galaxy to arrive at the absolute magnitude.

Our metallicity-luminosity relation is shown in Figure 6. The general trend is an increase in metallicity with luminosity over the full magnitude range of the data $M_B = -21$ to -12 . Using a bivariate linear least squares fitting technique, we first fit the data with the absolute magnitude as the independent variable, then fit the data with the metallicity as the independent variable. Our final linear fit is the mean of the two fits, which is described by the equation:

$$12 + \log(\text{O}/\text{H}) = 3.60 - 0.267M_B. \quad (7)$$

$$(\pm 0.20) \quad (\pm 0.009)$$

This is shown as the solid line in Figure 6. The scatter about the fit remains constant over the absolute magnitude range of $M_B = -21$ to -16 , with an RMS of 0.27 dex. The scatter is systematically one sided for $M_B > -16$, implying that there may be a shallower slope at the low metallicity end. The small formal errors in the coefficients of Equation 7 are somewhat deceiving. In arriving at these error bars we assumed an error in the absolute magnitude of 0.5 mags, which reflects the formal photometric errors, the uncertainty in the Hubble constant, and any possible peculiar velocities of the individual galaxies. An error in the metallicity of 0.16 dex is assumed, consistent with the scatter in the line diagnostic diagrams from which we estimate our metallicities. Because we have a large data set, these error estimates translate to very small formal errors in the slope and intercept of the fits. However, the difference in slopes from the direct and inverse fits of the bivariate fitting are substantially larger than the quoted uncertainty.

The slope we obtain is affected by two parameters. First, the choice of the R_{23} calibration affects the metallicities we derive for our Group II and therefore Group III data. Second, the absolute magnitude measurements may suffer from internal absorption. More massive galaxies are likely to have systematically higher extinction than dwarf galaxies due to their higher metallicities and higher dust content. This would, if left uncorrected, affect the slope of the metallicity-luminosity relation. We attempt to address both these issues.

There are several different calibrations relating R_{23} to metallicity at the high metallicity end. We chose the Edmunds and Pagel (1984) fit primarily because of its long standing use and simplicity. Pilyugin (2000) offers an updated R_{23} relation which takes into account data not available when Edmunds and Pagel made their original result. The Pilyugin relation is:

$$12 + \log(\text{O}/\text{H}) = 9.50 - 1.40 \cdot \log(R_{23}), \quad (8)$$

which is roughly parallel to but systematically lower than the Edmunds and Pagel fit by 0.07 dex. If we use this result to calibrate the upper branch of the R_{23} relation, we find the following metallicity-luminosity relation:

$$12 + \log(\text{O}/\text{H}) = 3.763 - 0.255M_B. \quad (9)$$

The derived slope is slightly shallower than when using the Edmunds and Pagel R_{23} relation. However, it remains much steeper than previous studies (see below). We conclude that while our result is somewhat dependent on the R_{23} calibration, any reasonable choice for R_{23} will give rise to a significantly steeper slope in the metallicity-luminosity relation, compared with the slopes derived for dwarf galaxies.

More problematic is quantifying the absorption caused by dust internal to a given galaxy. As massive galaxies tend to contain more dust, they suffer from internal absorption more than dwarf galaxies. Thus luminosities of massive galaxies are likely to be underestimated more than luminosities of dwarf galaxies. Correcting the measured absolute magnitudes for this internal extinction will make the slope of the metallicity-luminosity relation more shallow. As the imaging data do not in general reveal the Hubble type or axial ratio of the galaxies, traditional absorption corrections are not possible. We attempt a non-standard correction in the following way. A plot of B-V color vs. M_B for each galaxy shows a trend of increasing red colors with increasing luminosity. There is scatter in the trend due both to the variations in the stellar populations from galaxy to galaxy, as well as to the amount of internal reddening and absorption in the galaxy. We fit a line to the trend ignoring the most deviant red points which are most strongly affected by dust. The fit is taken to be the center of the color distribution in the absence of internal reddening. We then infer a color excess, $E(B-V)$, by measuring the color difference between each galaxy and the regression line. We assume that objects redder than 2σ from the mean regression line, and with $c_{H\beta}$ greater than 0.25, suffer from internal absorption. The deviant points are corrected to the trend line by assuming the following reddening law:

$$A_B = 4.0E(B - V) \quad (10)$$

While admittedly ad hoc, this absorption correction does systematically account for the most heavily extinguished galaxies in our sample. All of the galaxies that were corrected have $M_B < -16$ mags. The result of the correction on the metallicity-luminosity relation (using the Edmunds and Pagel R_{23} relation) is plotted in Figure 7. Once again a bivariate linear least squares fit is applied and we find the following result for the metallicity-luminosity relation:

$$12 + \log(\text{O}/\text{H}) = 4.059 - 0.240M_B, \quad (11)$$

$$(\pm 0.17) \quad (\pm 0.006)$$

with an RMS of 0.252.

After the extinction correction is applied to the data, we continue to find a slope steeper than those reported in the literature. Previous groups have concentrated on the low-metallicity, low-luminosity end where T_e abundances are available. Skillman et al. (1989) used metallicities from 20 nearby irregular galaxies, with absolute magnitudes between $M_B = -19$ to -10.5 , to study the metallicity-luminosity relation. They calculated metallicities from the T_e method and distances from Cepheid variables and group associations, and found $12 + \log(\text{O}/\text{H}) = 5.50 - 0.153M_B$ (dashed line in Figure 6), with an RMS deviation of 0.16 dex. Similarly, Richer and McCall (1995) report a

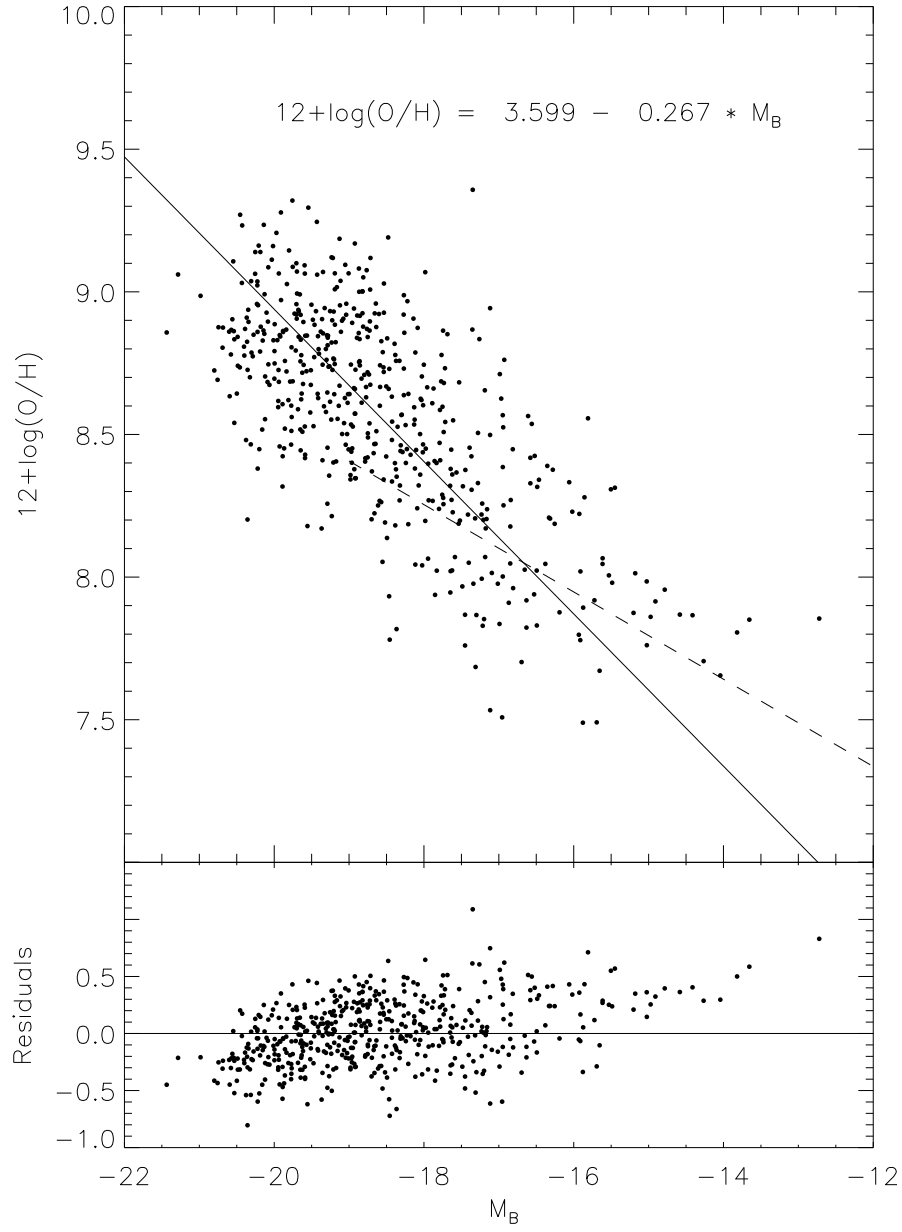


FIG. 6.— The metallicity-luminosity relationship is plotted in the top panel. The fit to the relationship is given as a solid line while the fit derived by Skillman et al. (1989) is shown as a dashed line. The bottom panel shows the residuals to the fit which have an RMS deviation of 0.27.

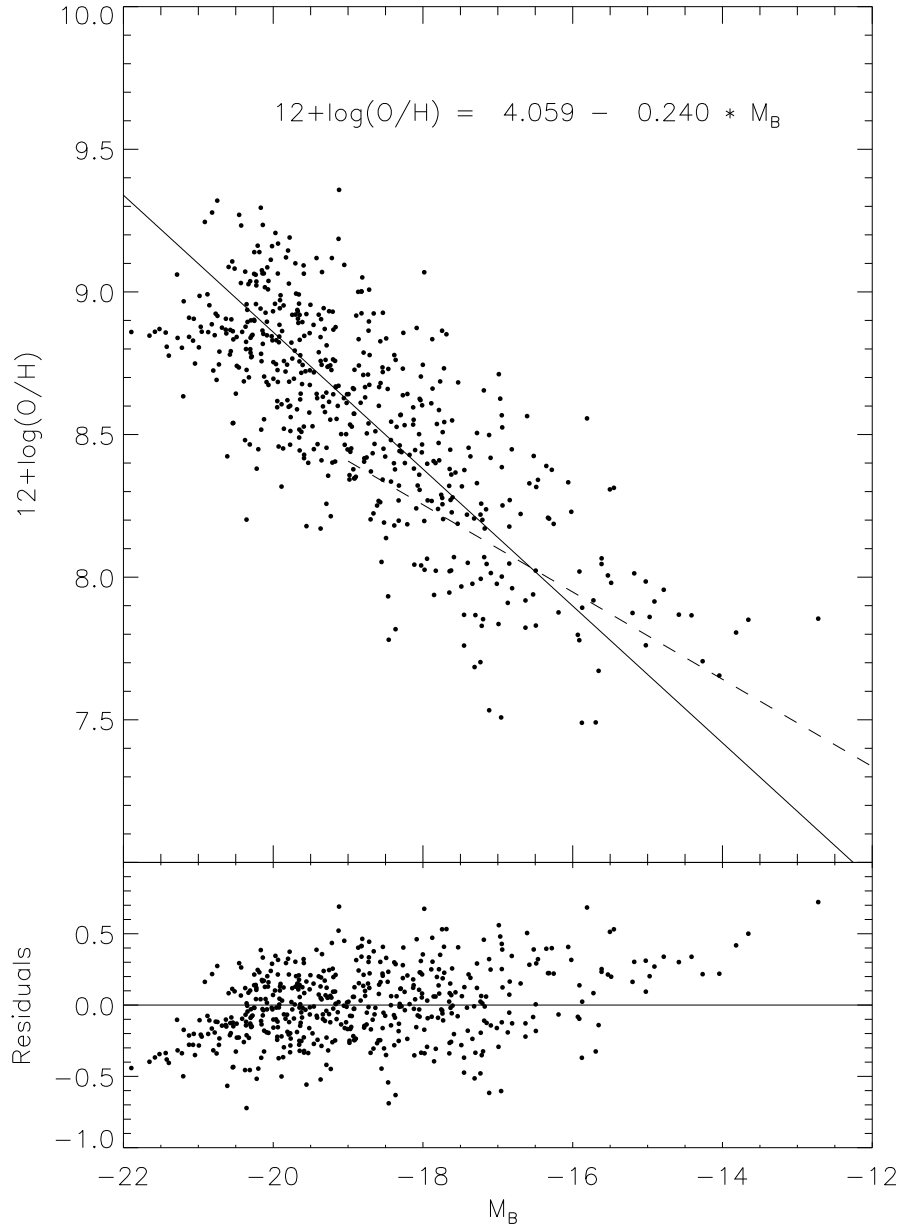


FIG. 7.— After correcting the luminosities for reddening and adopting the Pagel R_{23} relation, we arrive at the metallicity-luminosity relationship plotted in the top panel. The fit to the relationship is given as a solid line while the fit derived by Skillman et al. (1989) is shown as a dashed line. The bottom panel shows the residuals to the fit which have an RMS deviation of 0.25.

metallicity-luminosity relation for 18 nearby dwarf irregulars of $12 + \log(\text{O}/\text{H}) = (5.67 \pm 0.48) - (0.147 \pm 0.029)M_B$. Their data range in luminosity from $M_B = -18$ to -10.5 with a dispersion that increases for $M_B > -15$. Again, metallicities are derived from the T_e method and distances from stellar calibrators.

Until recently, published fits of the metallicity-luminosity relation have not included high luminosity galaxies in their samples. However, in looking back to data sets on the metallicity of large spirals such as Zaritsky et al. (1994) we find previous evidence for the fact that massive galaxies follow a steeper metallicity-luminosity relation than do dwarf galaxies. This is clear from Figure 13 of Zaritsky et al., where the data follow a steeper slope than the line included on the plot which has a slope similar to Skillman et al. When we combine the Zaritsky et al. data set (39 spirals) with the Skillman et al. data, we find a metallicity-luminosity relation given by $12 + \log(\text{O}/\text{H}) = 4.71 - 0.210M_B$. In another effort to combine the low luminosity results with high luminosity systems, Pilyugin and Ferrini (2000) combine the Richer and McCall data set with 13 objects from the Garnett et al. (1997) data set and include 17 objects from their own observations. These data, ranging in M_B from -21.5 to -10.5 , have a metallicity-luminosity relation with a slope of -0.192 . This is evidence that the overall slope may be steeper than indicated by the dwarfs alone, though still not as steep as our data indicate. One might well expect our data to give a steeper slope than the compilation of Pilyugin and Ferrini. The large spirals used in their data set have metallicities derived from several HII regions within the disk of each galaxy and averaged together. In contrast, our most metal rich galaxies tend to be starburst nucleus galaxies, where the emission is coming from a large star-forming event in the center of the galaxy. Because spirals are known to exhibit radial abundance gradients, nuclear starburst galaxies should as a group tend to have higher metallicities than those measured from disk HII regions, even for galaxies with similar luminosities. This is born out in a recent paper by Contini et al (2001). They plot a metallicity-luminosity relation for a large sample of galaxies. The irregular galaxies in their sample follow a metallicity-luminosity relation similar to Richer and McCall (1995). The larger HII galaxies and UV selected galaxies follow a linear relation with a higher slope of -0.173 . Displayed on their plot, but not included in either fit, is a large population of starburst nucleus galaxies. These galaxies tend to have luminosities similar to the UV selected galaxies but tend to have higher metallicities. It is clear that the inclusion of the starburst nucleus galaxies in a composite fit would lead to a significantly higher slope.

In conclusion, we believe that the steeper slope indicated by our data is reasonable. We stress, however, that this result is not meant to replace the work of Skillman et al. and others, but rather to investigate the metallicity-luminosity relationship with a wider sample of galaxy types. In fact Figure 7 shows evidence that the overall form of the relation may not be a simple linear function, but rather may be a higher order polynomial. The slope appears to become more shallow at the low luminosity end, resembling the slopes found by previous studies. Because of the large

scatter and relative paucity of galaxies at the low luminosity end, we do not feel we can adequately justify a higher-order fit with the current data set.

5. DISCUSSION AND CONCLUSIONS

The metallicity-luminosity relation has significant implications for galaxian evolution. It appears to be a continuous smooth function from high-luminosity massive spirals to the low-luminosity dwarf galaxies, implying that the metallicity-luminosity relation is at work on all mass scales and all galaxy types with significant star formation. The form of the metallicity-luminosity relation, along with its intrinsic scatter, should provide a useful constraint for theoretical models of chemical evolution in galaxies.

We have confirmed the existence of the metallicity-luminosity relationship using data from 519 starburst galaxies. We found a linear relation between metallicity and absolute B magnitude given by: $12 + \log(\text{O}/\text{H}) = 4.059 - 0.240M_B$. Metallicities were derived for the large sample from secondary metallicity indicators relating the strong nebular lines, $[\text{OIII}]\lambda 5007$ and $[\text{NII}]\lambda 6583$, to metallicity. We used T_e abundances from 12 galaxies, p_3 abundances for 13 galaxies and R_{23} abundances for 46 galaxies, to relate emission-line ratios with metallicity. This study uses the largest sample of galaxies to date to construct a metallicity-luminosity relation. We find a significantly steeper slope than previous results, most likely due to the fact that we probe to higher luminosities and include a more diverse mix of galaxy types in our sample. The large scatter, 0.252 dex, remains roughly constant to an absolute magnitude of $M_B = -16$, at which point the scatter becomes one sided. This indicates that the slope may be more shallow at the low luminosity end, in agreement with previous results that have focused on dwarf systems. Interestingly, Richer and McCall have also found the scatter in their metallicity-luminosity relation to be one sided for objects with $M_B > -16$. This may be further evidence for the need of higher order fits to the relation. We have resisted the urge to carry out a higher order fit to the data due to the large intrinsic scatter in our sample.

In interpreting the results illustrated in Figure 7, the reader should keep in mind the following cautionary note. As mentioned above, the abundances we measure for the more luminous KISS galaxies are predominantly central/nuclear values, rather than disk HII regions. Since spiral galaxies typically exhibit radial abundance gradients, our abundances may be biased to higher values compared to previous studies. Clearly, one needs to consider the location within the galaxy when quoting abundances (particularly for large spirals) and investigating the metallicity-luminosity relation. While there is no absolute correct method or convention, we would argue that our use of nuclear abundances is no less appropriate than using outlying disk HII regions (which will be biased to lower abundances). In fact, since dwarf galaxies tend to exhibit no substantial abundance gradients, the use of central abundance measurements might well be preferred.

We have investigated whether this effect could be the cause for our steeper metallicity-luminosity relation by comparing our results with those from previous studies. For example, the large dataset of Zaritsky et al. (1994), derived from disk HII regions rather than nuclear star-

forming regions, exhibits a metallicity-luminosity relation very similar to ours at $M_B < -18$. No bias is evident when the two datasets are compared directly. This may be due in part to the fact that many spiral galaxies exhibit only very shallow abundance gradients (or in some cases none at all). We conclude that our use of central abundances is not the main cause for our steep metallicity-luminosity relation, but rather that this is a real phenomenon. We point out that evidence for a steeper slope to the metallicity-luminosity relation has been available but not pursued until Pilyugin and Ferrini (2000) combined the Garnett et al. and Richer and McCall data sets to observe the overall trend. Their study found a slope steeper than those indicated by Skillman et al. and Richer and McCall. Seeking further confirmation of this result, we combined data from Zaritsky et al. (39 spirals) with data from Skillman et al. We again found evidence for a steeper slope. The metallicity-luminosity relation using this data set is given by: $12 + \log(\text{O}/\text{H}) = 4.71 - 0.210 M_B$.

The KISS sample of galaxies includes a diverse mass and morphology range, from blue compact dwarfs to giant nuclear starburst galaxies. By including the more massive galaxies and achieving a large sample, we appear to be observing a more general metallicity-luminosity trend than is indicated by the dwarf galaxies alone. While the metallicity-luminosity relation derived by Skillman et al. appears to be a good approximation of the low metallicity data, extrapolating their relation to higher luminosities is probably inappropriate. Efforts to understand the physical mechanisms that lead to the observed metallicity-luminosity relation will be aided by the constraints set by the data presented in this paper.

The methods used here to calculate coarse metal abun-

dances allow for a way to quickly identify low metallicity candidates for further study. The KISS galaxies believed to be low metallicity will be targeted as high priority systems for abundance quality spectra in future observing runs. Eventually this will yield a large number of low metallicity objects that can be used to place constraints on the primordial helium abundance of the Universe. The coarse abundance methods can also be applied to galaxies at higher redshift, where $[\text{OIII}]\lambda 4363$ is difficult to observe. Metallicity comparisons between galaxies over a range of redshifts will help to shed light on the chemical evolution of galaxies.

We gratefully acknowledge financial support for the KISS project from an NSF Presidential Faculty Award to JJS (NSF-AST-9553020), as well as continued support for our ongoing follow-up spectroscopy campaign (NSF-AST-0071114). We also thank Wesleyan University for providing additional funding for several of the observing runs during which the spectral data were obtained. We are grateful to the anonymous referee for many suggestions which improved the quality of this paper. We thank the numerous KISS team members who have participated in the spectroscopic follow-up observations during the past several years, particularly Caryl Gronwall, Drew Phillips, Gary Wegner, Laura Chomiuk, Kerrie McKinstry, Robin Ciardullo, Jeffrey Van Duyne and Vicki Sarajedini. Finally, we wish to thank the support staffs of Kitt Peak National Observatory, Lick Observatory, the Hobbey-Eberly Telescope, MDM Observatory, and Apache Point Observatory for their excellent assistance in obtaining these observations.

REFERENCES

- Contini, T., Treyer, M. A., Sullivan, M. & Ellis, R. S. 2001, MNRAS, in press (astro-ph/0109395)
- de Robertis, M. M., Dufour, R. J., & Hunt, R. W. 1987, JRASC, 81, 195
- Edmunds, M. G., & Pagel, B. E. J. 1984, MNRAS, 211, 507
- Garnett, D. R., Shields, G. A., Skillman, E. D., Sagan, S. P., & Dufour, R. J. 1997, ApJ, 489, 63
- Gronwall, C., Salzer, J. J., Sarajedini, V. L., Chomiuk, L. B., Moody, J. W., Frattare, L. M., & Boroson, T. A. 2002a, in preparation
- Gronwall, C., Salzer, J. J., Jangren, A., Wegner, G. A., Phillips, A. C., Melbourne, J., Ciardullo, R., & McKinstry, K. 2002b, in preparation
- Hidalgo-Gamez, A. M., & Olofsson, K. 1998, A&A, 334, 45
- Hunter, D. A., & Hoffman, L. 1999, AJ, 117, 2789
- Izotov, Y. I., Thuan, T. X., & Lipovetsky, V. A. 1994, ApJ, 435, 647
- Izotov, Y. I., Thuan, T. X., & Lipovetsky, V. A. 1997, ApJSS, 108, 1
- Izotov, Y. I., & Thuan, T. X. 1998, ApJ, 500, 188
- Izotov, Y. I., & Thuan, T. X. 1999, ApJ, 511, 639
- Mac Low, M., & Ferrara, A. 1999, ApJ, 513, 142
- McGaugh, S. S. 1991, ApJ, 380, 140
- Melbourne, J., Phillips, A. C., Salzer, J. J., Gronwall, C., & Sarajedini, V. L. 2002, in preparation
- Osterbrock, D. E. 1989, *Astrophysics of Gaseous Nebulae and Active Galactic Nuclei* (University Science Books, Mill Valley, CA)
- Pagel, B. E. J., Edmunds, M. G., Blackwell, D. E., Chun, M. S., & Smith, G. 1979, MNRAS, 189, 95
- Pilyugin, L. S. 2000, A&A, 362, 325
- Pilyugin, L. S. 2001a, A&A, 369, 594
- Pilyugin, L. S. 2001b, A&A, 374, 412
- Pilyugin, L. S., & Ferrini, F. 2000, A&A, 358, 72
- Richer, M. G., & McCall, M. L. 1995, ApJ, 445, 642
- Ryder, S. D. 1995, ApJ, 444, 610
- Salzer, J. J., Gronwall, C., Lipovetsky, V. A., Kniazev, A., Moody, J. W., Boroson, T. A., Thuan, T. X., Izotov, Y. I., Herrero, J. L., & Frattare, L. M. 2000, AJ, 120, 80
- Salzer, J. J., Gronwall, C., Lipovetsky, V. A., Kniazev, A., Moody, J. W., Boroson, T. A., Thuan, T. X., Izotov, Y. I., Herrero, J. L., & Frattare, L. M. 2001, AJ, 121, 66
- Salzer, J. J., Gronwall, C., Sarajedini, V. L., Lipovetsky, V. A., Kniazev, A., Moody, J. W., Boroson, T. A., Thuan, T. X., Izotov, Y. I., Herrero, J. L., & Frattare, L. M. 2002a, AJ, 123, in press
- Salzer, J. J., Gronwall, C., Jangren, A., & McKinstry, K. 2002b, in preparation
- Shaw, R. A., & Dufour, R. J. 1995, PASP, 107, 896
- Skillman, E. D., Kennicutt, R. C., & Hodge, P. W. 1989, ApJ, 347, 875
- Vila-Costas, M. B., & Edmunds, M. G. 1992, MNRAS, 259, 121
- Wegner, G. A., Salzer, J. J., Gronwall, C., Jangren, A., & Melbourne, J. 2002, in preparation
- Zaritsky, D., Kennicutt, R. C., & Huchra, J. P. 1994, ApJ, 420, 87

TABLE 1
METAL ABUNDANCES FROM THE T_e METHOD.

KISSR ^a	$\log([\text{OII}]/\text{H}\beta)$	$\log([\text{OIII}]/\text{H}\beta)$ ^b	$12 + \log(\text{O}/\text{H})$
49	0.619	0.670	8.00
85	0.024	0.658	7.50
396	0.413	0.759	7.90
666	-0.310	0.913	7.54
675	0.145	0.878	7.78
1013	0.438	0.829	7.72
1194	0.311	0.834	7.95
1490	0.179	0.715	7.54
1752	0.038	0.678	7.56
1778	0.466	0.599	7.93
1845	0.393	0.847	8.04
KISSB ^c	$\log([\text{OII}]/\text{H}\beta)$	$\log([\text{OIII}]/\text{H}\beta)$ ^b	$12 + \log(\text{O}/\text{H})$
23	0.430	0.448	7.50

^aThis is the running number for the galaxy as listed in Salzer et al. 2001.

^b $[\text{OIII}]\lambda 4959 + \lambda 5007/\text{H}\beta$

^cThis is the running number for the galaxy as listed in Salzer et al. 2002a.

TABLE 2
METAL ABUNDANCES FROM THE R_{23} METHOD.

KISSR	$\log([\text{OII}]/\text{H}\beta)$	$\log([\text{OIII}]/\text{H}\beta)^{\text{a}}$	$12 + \log(\text{O}/\text{H})$
1	0.651	0.249	8.47
3	0.729	-0.044	8.47
68	0.426	0.538	8.48
91	0.549	0.291	8.55
109	0.506	0.326	8.57
110	0.434	0.016	8.78
117	0.484	0.499	8.48
124	0.506	0.497	8.46
145	0.420	-0.110	8.84
185	0.355	-0.093	8.90
257	0.562	0.433	8.46
265	0.489	0.389	8.54
292	0.522	0.605	8.37
317	0.404	0.637	8.42
322	-0.043	-0.439	9.43
326	0.631	0.120	8.54
327	0.580	0.472	8.42
333	0.430	-0.188	8.85
335	0.386	0.358	8.64
343	0.415	0.824	8.24
368	0.711	-0.171	8.52
398	0.501	-0.020	8.72
400	0.371	-0.239	8.93
515	0.524	0.067	8.67
520	0.440	-0.032	8.79
577	0.572	-0.110	8.67
582	0.759	0.472	8.27
595	0.005	-0.803	9.48
610	0.461	0.202	8.67
643	0.505	0.441	8.50
830	0.690	0.386	8.38
833	0.566	0.001	8.64
894	0.614	-0.044	8.60
910	0.416	0.063	8.78
1016	0.502	-0.006	8.72
1028	-0.092	-0.472	9.49
1032	0.520	0.295	8.57
1055	0.550	-0.145	8.70
1062	0.565	0.345	8.51
1402	0.571	-0.509	8.73
1416	0.615	0.325	8.47
1424	0.490	-0.247	8.79
1537	0.522	0.510	8.44
1885	0.364	0.237	8.73
1940	0.626	0.321	8.46
2021	0.564	0.084	8.62

^a $[\text{OIII}]\lambda 4959 + \lambda 5007/\text{H}\beta$

TABLE 3
METAL ABUNDANCES FROM THE p_3 METHOD.

KISSR	$\log([\text{OII}]/\text{H}\beta)$	$\log([\text{OIII}]/\text{H}\beta)^{\text{a}}$	$12 + \log(\text{O}/\text{H})$
96	0.280	0.851	7.91
97	0.493	0.753	8.05
105	0.166	0.592	7.65
120	0.167	0.800	7.80
272	0.359	0.601	7.85
310	-0.097	0.929	7.82
311	0.248	0.794	7.85
404	0.459	0.581	7.97
405	0.154	0.580	7.63
528	0.507	0.707	8.05
785	0.287	0.885	7.95
803	0.600	0.632	8.18
1794	0.322	0.736	7.87

^a $[\text{OIII}]\lambda 4959 + \lambda 5007/\text{H}\beta$

TABLE 4
GALAXIES WITH ESTIMATED METALLICITIES BELOW 7.9 DEX.

KISSR	$\log([\text{OIII}]/\text{H}\beta)^{\text{a}}$	$\log([\text{NII}]/\text{H}\alpha)^{\text{b}}$	$12 + \log(\text{O}/\text{H})$
55	0.808	-1.654	7.78
73	0.623	-1.531	7.85
85	0.533	-1.686	7.76
105	0.467	-1.502	7.87
272	0.476	-1.528	7.85
310	0.804	-2.281	7.51
311	0.669	-1.799	7.70
396	0.634	-1.515	7.86
404	0.456	-1.489	7.88
405	0.455	-1.503	7.87
471	0.676	-2.340	7.49
666	0.788	-2.345	7.49
675	0.753	-1.688	7.76
698	0.844	-1.577	7.82
785	0.760	-1.565	7.83
799	0.690	-1.566	7.83
803	0.507	-1.505	7.87
885	0.727	-1.834	7.68
986	0.619	-2.202	7.53
1194	0.709	-1.506	7.87
1490	0.590	-1.606	7.81
1752	0.553	-1.896	7.66
1794	0.612	-1.492	7.87
KISSB	$\log([\text{OIII}]/\text{H}\beta)^{\text{a}}$	$\log([\text{NII}]/\text{H}\alpha)^{\text{b}}$	$12 + \log(\text{O}/\text{H})$
15	0.607	-1.556	7.84
23	0.323	-1.525	7.85
35	0.873	-1.651	7.78
41	0.786	-1.620	7.80
47	0.710	-1.792	7.71
53	0.660	-1.861	7.67
61	0.656	-1.586	7.82
66	0.770	-1.463	7.89

^a $[\text{OIII}]\lambda 5007/\text{H}\beta$

^b $[\text{NII}]\lambda 6583/\text{H}\alpha$